J. Iron Steel Res. Int. (2020) 27:169–179
https://doi.org/10.1007/s42243-019-00354-3

ORIGINAL PAPER

# High-performance chromite by structure stabilization treatment

**En-hui Wang[1] · Chang Luo[1] · Jun-hong Chen[2] · Xin-mei Hou[1]**

Received: 20 September 2018 / Revised: 21 November 2018 / Accepted: 4 December 2018 / Published online: 8 January 2020


**Abstract**
Chromite is an important raw material applied in refractories. Efforts have been made to obtain high-performance chromite by adding MgO and $Al_2O_3$ from the viewpoint of structure optimization. In order to explore the effect of $Al_2O_3$ and MgO on the structure, two formulas, i.e., Mg-rich and Al-rich ones, were selected. The phase and microstructure development of samples heated in the temperature range of 1200–1600 °C were studied by X-ray diffraction and scanning electron microscopy with energy-dispersive spectrometry. MgO and $Al_2O_3$ added have diffused into chromite successfully by heat treatment. MgO diffuses into chromite, occupying the tetrahedral vacancies caused by the diffusion and oxidation of $Fe^{2+}$ ions to stabilize the structure. $Al_2O_3$ diffuses into the surface layer of chromite, forming spinel-sesquioxide structure. Al-rich sample which has spinel-sesquioxide structure shows better corrosion resistance toward fayalite slag than Mg-rich sample which has single spinel structure by blocking the interdiffusion between $Fe^{2+}$ ions in fayalite slag and $Mg^{2+}$ ions in chromite.

**Keywords** Chromite · Structure optimization · Corrosion resistance · Refractory

## 1 Introduction

Magnesia–chromite bricks are widely applied in nonferrous furnaces, especially in copper converter [1]. Usually, they can be divided into three types, i.e., direct-bonded, rebounded and semi-rebounded [2]. Magnesia–chromite bricks as refractories usually adopt pre-synthesis fused chromite magnesite, chromite and magnesia as raw materials. The pre-synthesis fused chromite magnesite adopted has complex synthetic process and high costs, which brings environmental and energy problems. By comparison, natural chromite is a promising candidate of pre-synthesis fused chromite magnesite because of its high $Cr_2O_3$ content and spinel structure which is beneficial to slag resistance [3]. The structure of chromite is a solid solution of $FeCr_2O_4$, $Fe_3O_4$, $FeAl_2O_4$, $MgCr_2O_4$, $MgFe_2O_4$ and $MgAl_2O_4$ pure spinel end numbers [1], and thus, it has a formula unit of $(Mg,Fe^{2+})[Cr,Al,Fe^{3+}]_2O_4$. The cation arrangement of chromite is that $Mg^{2+}$, $Fe^{2+}$ and $Fe^{3+}$ ions fill tetrahedral sites and $Cr^{3+}$ and $Al^{3+}$ ions occupy octahedral sites. It is well known that industrial chromite is difficult to sinter and may undergo many changes during sintering. When exposed to oxidizing atmosphere, tetrahedral vacancies are produced due to the diffusion of ferrous ions, which causes the unstable spinel structure. Thus, chromite undergoes some volume expansion and strength loss after firing [4]. When contacting fayalite slag, $Fe^{2+}$ ions in slag substitute $Mg^{2+}$ ions in chromite, leading to the formation of Fe-rich spinel. Overmuch Fe-rich spinel will cause structure spalling during the employment in copper industries because of the fluctuation of temperature and atmosphere. To overcome the disadvantage of chromite, structure optimization is of most importance. Some researchers tried to add excess MgO, aiming to make iron oxides stable [2, 5, 6]. However, the corrosion usually occurs because of the dissolution of MgO when contacting fayalite slag [7]. Some researchers pointed out that $Al_2O_3$ is an important component to be added to enhance spalling resistance of chromite [2]. Zhu et al. [8] analyzed the influence of α-$Al_2O_3$ micropowder addition on the high-temperature properties of magnesia chrome materials. It was found that 6% α-$Al_2O_3$ micropowder addition can improve

En-hui Wang and Chang Luo have contributed equally to this work.

✉ Xin-mei Hou
houxinmeiustb@ustb.edu.cn

[1] Collaborative Innovation Center of Steel Technology, University of Science and Technology Beijing, Beijing 100083, China

[2] School of Materials Science and Engineering, University of Science and Technology Beijing, Beijing 100083, China

the comprehensive performance of magnesia chromite material. However, Al-rich chromite is less corrosion resistant [9].

In essence, the performance of chromite is improved mainly based on the structural optimization. In this work, the phase and morphological development of chromite during sintering are investigated by introducing MgO and $Al_2O_3$ as additives from the viewpoint of structural optimization. Their slag resistance is further investigated. This can lay basic foundation for the wide application of chromite as raw materials of high-performance magnesia–chromite bricks.

## 2 Structure stabilization theory

The main chemical changes of chromite during firing in air are as follows [10]: (1) From 820 to 1170 °C, the imposed oxygen chemical potential promotes the outward diffusion of $Fe^{2+}$ ions from the core of chromite crystals and $Fe^{2+}$ ions are oxidized into $Fe^{3+}$. A new anion lattice is created along with the cationic vacancies. The vacancies generated diffuse inward and promote the outward diffusion of cations, leading to the formation of an Fe-rich maghemite-type ($(Fe^{3+})[Fe^{3+}_{5/6\square 1/6}]_2O_4$) defective metastable spinel near the surface. (2) From 1240 to 1370 °C, dissociation of $Fe_2O_3$ to $FeO{\cdot}xFe_2O_3$ occurs, and the spinel phase formed then redissolves in the chromite spinel solid solution matrix. The cationic vacancies produced during firing process provide pathway for the additives to diffuse into chromite grains.

To optimize the structure of chromite, two key points should be taken into consideration. One is to maintain the structure stability during the sintering process caused by the diffusion and oxidation of $Fe^{2+}$, and the other is to exhibit excellent erosion resistance toward fayalite slag. The instability of chromite is mainly caused by the tetrahedral vacancies. Therefore, the bivalent metal cations can be introduced to occupy the tetrahedral vacancies. As a common bivalent metal oxide, magnesia is widely applied [11]. In view of the excellent erosion resistance toward fayalite slag, spinel-sesquioxide structure can meet above requirement. Sesquioxide is the general terms of trivalent metal oxide such as $Cr_2O_3$, $Al_2O_3$ and $Fe_2O_3$ [12]. Different from the spinel structure, sesquioxide belongs to trigonal system where $M^{3+}$ ions fill the octahedral sites between the oxygen anions. The diffusion of $Fe^{2+}$ into sesquioxide is blocked due to the prolongation of diffusion path compared with the single spinel structure; thus, the corrosion resistance is improved. Meanwhile, sesquioxide can react with FeO from fayalite slag to form high melting point compound, which protects the chromite from being further corroded. To form the above structure, $Al_2O_3$ is usually adopted [12, 13].

It is right that the dissolution rate of MgO and $Al_2O_3$ in fayalite slag is fast, and even $MgAl_2O_4$ spinel is unable to meet the requirement. However, in the current experiment, the existing form of MgO is neither single MgO phase nor $MgAl_2O_4$ spinel, and it exists as chromite spinel, in which $Mg^{2+}$ has to pass through a longer distance for dissolution and thus possesses lower reactivity compared with MgO and $MgAl_2O_4$. Meanwhile, $Al_2O_3$ added can form sesquioxide phase which contains $Fe^{3+}$ and $Cr^{3+}$, and the reactivity of $Al_2O_3$ in this sesquioxide is much lower too. Therefore, it is assumed that the performance of chromite by introducing MgO and $Al_2O_3$ as additives can be improved.

## 3 Experimental

South Africa chromite (~100 μm), commercial Chinese fused magnesia (~5.2 μm) and α-$Al_2O_3$ (~4.8 μm) purchased from Luzhong, Shandong province, China, were adopted as raw materials, and their compositions are listed in Table 1. In order to explore the effect of $Al_2O_3$ and MgO on the structure, two formulas, i.e., Mg-rich and Al-rich ones, were selected. In view of Mg-rich sample, the mass percent of chromite, MgO and $Al_2O_3$ is 80%, 10% and 10%, while the mass percent in Al-rich sample is 80%, 2% and 18%, respectively. The sample can be named as Mg-rich and Al-rich samples for simplification.

The mixture of chromite, MgO and $Al_2O_3$ was stirred with moderate deionized water to gain stable slurry. The as-received suspensions were poured into 10 mm × 10 mm × 40 mm molds and dried at room temperature for 24 h. After being demolded, the samples were dried at 110 °C for further desiccation. Finally, the samples were heated in an electric furnace to 1200, 1300, 1400, 1500 and 1600 °C, respectively, at a heating rate of 5 °C/min in air and held for 4 h.

The crucibles for corrosion test are 40 mm in length, 40 mm in width and ~50 mm in height with a cylindrical hole of 18 mm in diameter and 30 mm in depth in the center.

**Table 1** Chemical composition of raw materials (mass%)

| Raw material | $Cr_2O_3$ | MgO | CaO | $Al_2O_3$ | $Fe_2O_3$ | $SiO_2$ | FeO |
|---|---|---|---|---|---|---|---|
| Chromite | 46.53 | 9.52 | _ | 15.33 | 7.36 | 0.97 | 20.28 |
| α-$Al_2O_3$ | _ | _ | 0.09 | 99.70 | 0.03 | 0.03 | _ |
| Magnesia | _ | 97.05 | 1.22 | 0.10 | 0.77 | 0.56 | _ |

The fayalite slag was synthesized in the experiment, and it is composed of pure $Fe_2SiO_4$, as shown in Fig. 1. The powder of synthetic fayalite slag was pressed into the hole. The slag resistance experiment was carried out at 1350 °C at a heating rate of 5 °C/min in argon atmosphere and held for 2 h.

The permanent linear change was measured and the cold modulus of rupture values was also measured using the three-point bending test. The composition of the specimens was identified using X-ray diffractometer (XRD, D8 Advance, Bruker, Germany) in the scanning range of 10°–90°. The microstructure was analyzed using a scanning electron microscope (SEM, novaTM nano 450, FEI Company, Hillsboro, OR, USA) equipped with an energy-dispersive spectrometer (EDAX-TEAM, EDAX, Mahwah, NJ, USA).

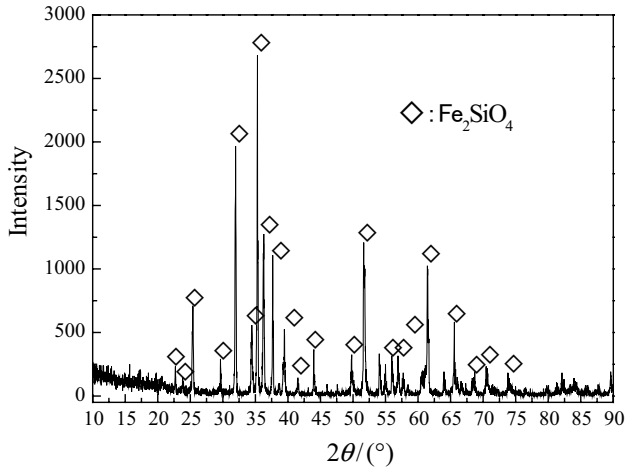


**Fig. 1** X-ray diffraction pattern of synthetic fayalite slag

## 4 Results and discussion

### 4.1 Phase and microstructure analysis of Mg-rich sample

Figure 2a shows the XRD patterns of Mg-rich sample heated at different temperatures. It can be seen that $Mg(Fe_yAl_{1-y})_2O_4$ spinel as a new phase appears in the samples fired at 1200, 1300 and 1400 °C besides chromite spinel because of the high diffusion rate of MgO in $Fe_2O_3$ [14]. Their values of $Mg(Fe_yAl_{1-y})_2O_4$ increase from 0.6 at 1200 to 1.2 at 1400 °C according to the interplanar spacing of (440) (Fig. 2b), indicating that more Fe ions diffuse outward from core with temperature rising [15]. With temperature further increasing to 1500 °C, $Mg(Fe_yAl_{1-y})_2O_4$ is not favorable because of the lower Gibbs free energy of $MgAl_2O_4$ and $MgCr_2O_4$ than that of $MgFe_2O_4$. $Mg^{2+}$ diffuses into the tetrahedral vacancies in the core of chromite, leaving $Fe_2O_3$ together with $Al_2O_3$ and $Cr_2O_3$ to form a new phase, i.e., sesquioxide. The interplanar spacing of (104) of sesquioxide can be calculated according to the Bragg equation:

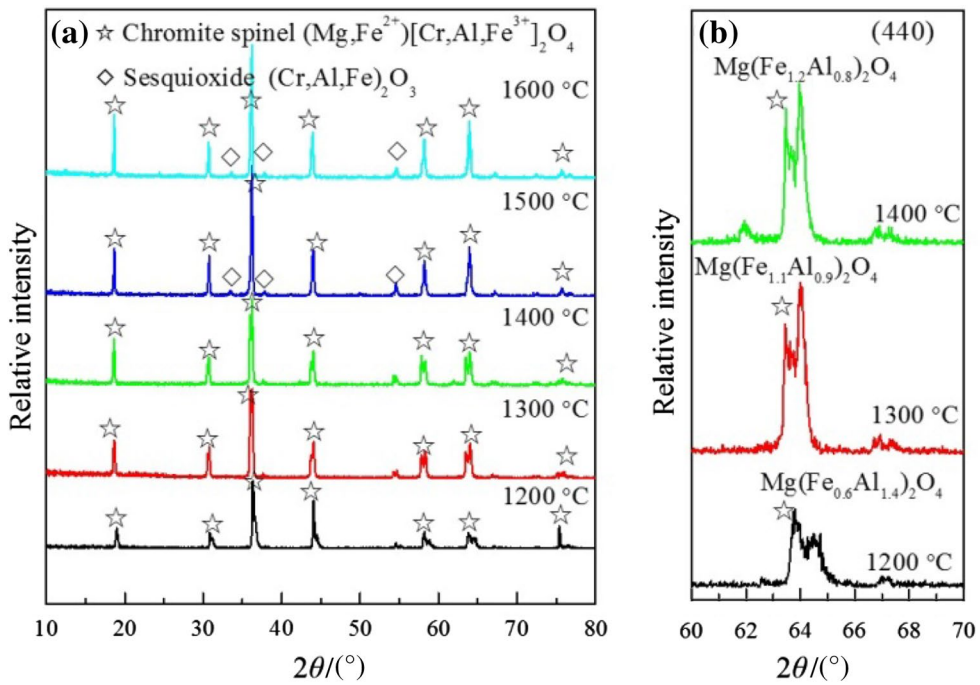


**Fig. 2** XRD patterns of Mg-rich sample heated in air at different temperatures (**a**) and (440) peak of $Mg(Fe_yAl_{1-y})_2O_4$ spinel heated at 1200, 1300 and 1400 °C (**b**)

$$d = \frac{n\lambda}{2\sin\theta} \quad (1)$$

where $d$ is the interplanar spacing; $n$ is the diffraction order; $\lambda$ is the wavelength of X-ray; and $\theta$ is the angle between the X-ray and the corresponding crystal face. The interplanar spacing can be calculated to be 0.26793 nm at 1500 °C and 0.26635 nm at 1600 °C, and the large $d$ value indicates that Fe-rich sesquioxide is formed [16].

Figure 3 shows the microstructure of cutting surface of Mg-rich sample fired at different temperatures. At low temperature, chromite particles (bright white) are randomly distributed and isolated by MgO particles (gray in picture), as shown in Fig. 3a, b. When heated at 1400 °C, some chromite particles begin to bond together due to the diffusion of ions, as shown in Fig. 3c. The interdiffusion of ions becomes more obvious at 1500 °C (Fig. 3d).

The element map scanning of Mg-rich sample was further analyzed. Figure 4a shows that there are some Mg concentration areas in sample heated at 1200 °C, indicating that most MgO added does not react. At the edge of chromite grain, there is an enrichment area of Mg, Al and Fe shown in Fig. 4a, indicating the new formation of $Mg(Fe_yAl_{1-y})_2O_4$ spinel verified by XRD (Fig. 2a). After heated at 1400 °C, the distribution of Mg becomes uniform shown in Fig. 4b, indicating that the diffusion of Mg to chromite has finished. The distribution of Fe is obviously more uniform than that of Cr, indicating that rising temperature contributes to the diffusion of Fe ions. The diffusion and oxidation of Fe lead to the formation of Fe-rich sesquioxide shown in Fig. 2a.

### 4.2 Phase and microstructure analysis of Al-rich sample

Figure 5a shows the XRD patterns of Al-rich sample heated at different temperatures. It can be seen that sample fired at 1200 °C contains chromite spinel, $Mg(Fe_{0.9}Al_{1.1})_2O_4$ and unreacted $Al_2O_3$. As temperature reaches 1300 °C, $Mg(Fe_{1.2}Al_{0.8})_2O_4$ spinel and sesquioxide appear. Fe content in $Mg(Fe_xAl_{1-x})_2O_4$ spinel increases when temperatures rise from 1200 to 1300 °C, indicating that higher temperature contributes to the diffusion of Fe ions. Sesquioxide appears at 1300 °C due to the excess trivalent oxides ($Cr_2O_3$, $Fe_2O_3$ and $Al_2O_3$) over divalent oxide (MgO and FeO) in chromite spinel. Above 1400 °C, chromite spinel and sesquioxide mainly exist due to the

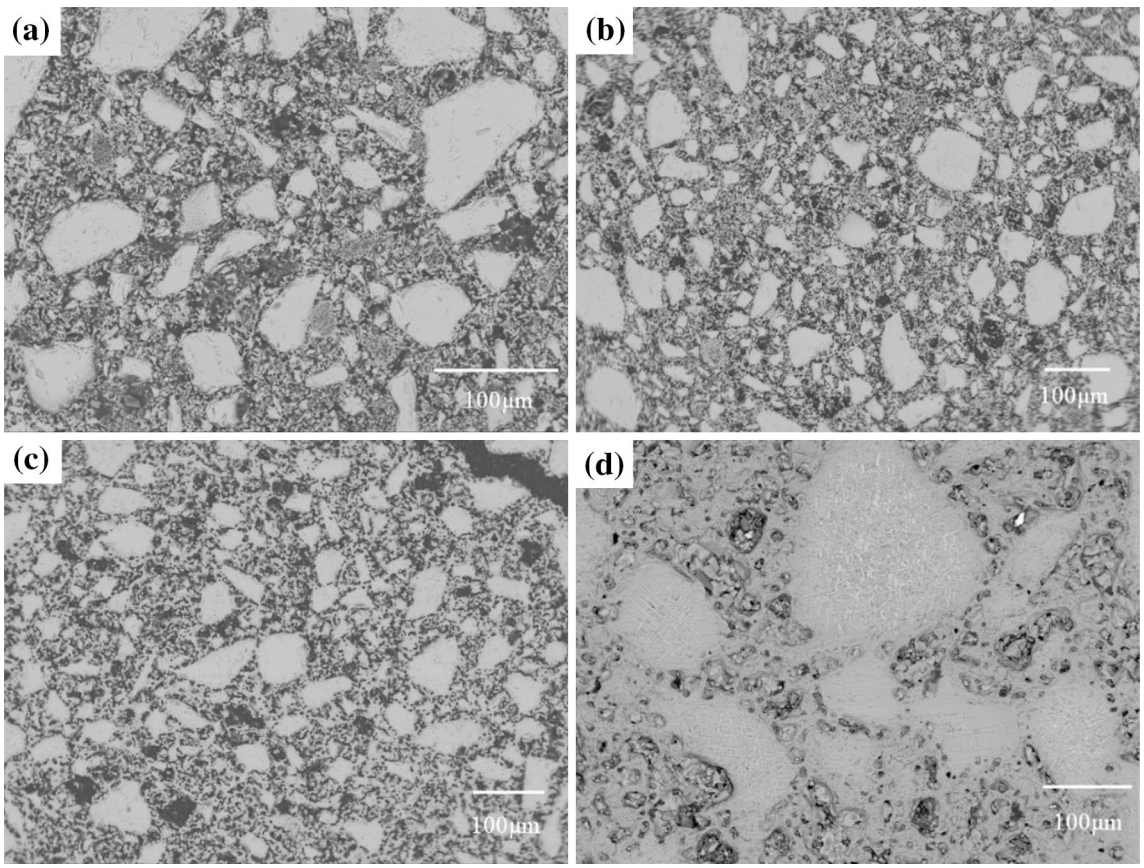


**Fig. 3** Microstructure of Mg-rich sample heated at 1200 °C (**a**), 1300 °C (**b**), 1400 °C (**c**) and 1500 °C (**d**)

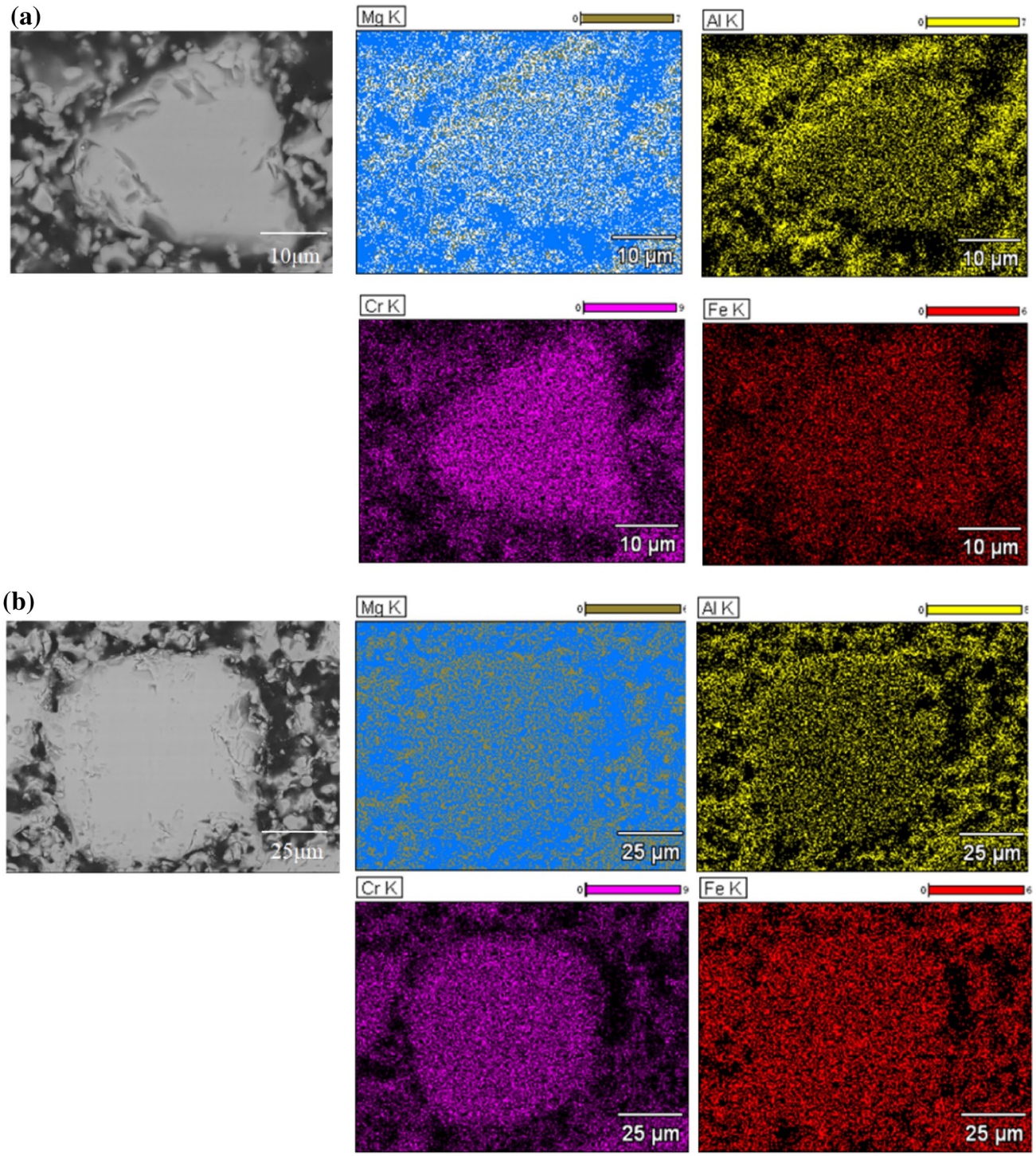


**Fig. 4** Element map scanning of Mg-rich sample heated at 1200 °C (**a**) and 1400 °C (**b**)

further diffusion of Mg ions into inner of chromite. The interplanar spacing of (104) of the sesquioxide (Fig. 5b) is calculated to increase from 0.25997 nm at 1300 °C to 0.26137 nm at 1600 °C, which is resulting from the ascent of Fe content in sesquioxide [17]. However, in general, the obtained sesquioxide is Al-rich compared with Mg-rich sample (Fig. 2) due to the smaller *d* value of (104), confirming that $Al^{3+}$ ions diffuse into the chromite.

Figure 6 shows the microstructure of cutting surface of the Al-rich sample heated at different temperatures. At low temperature, the chromite particles remain irregular (Fig. 6a), indicating that there is nearly no reaction

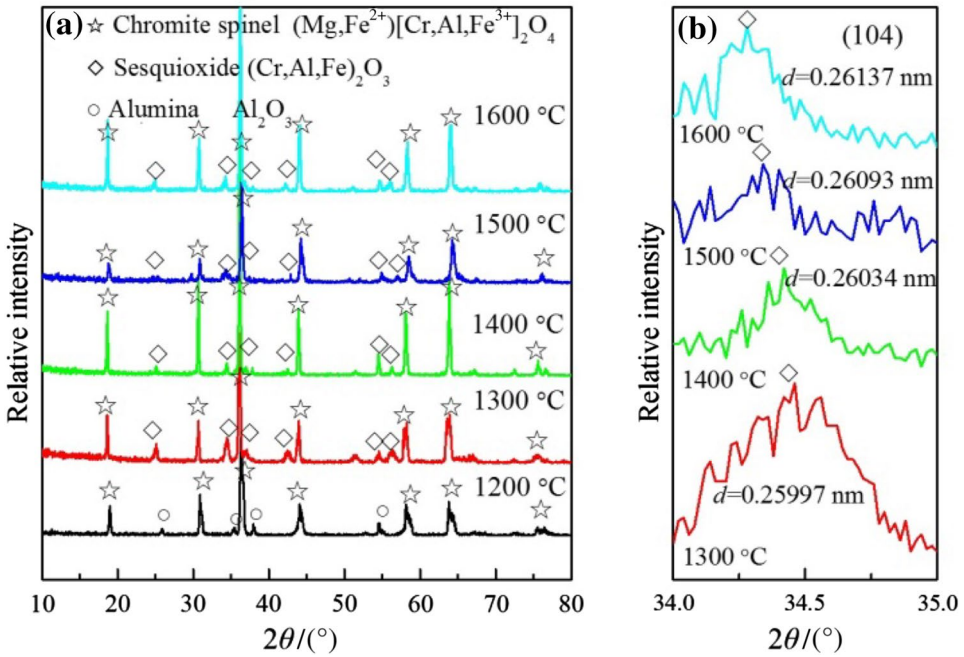


**Fig. 5** XRD patterns of Al-rich sample heated in air at various temperatures (**a**) and (104) peak of sesquioxide heated at different temperatures (**b**)

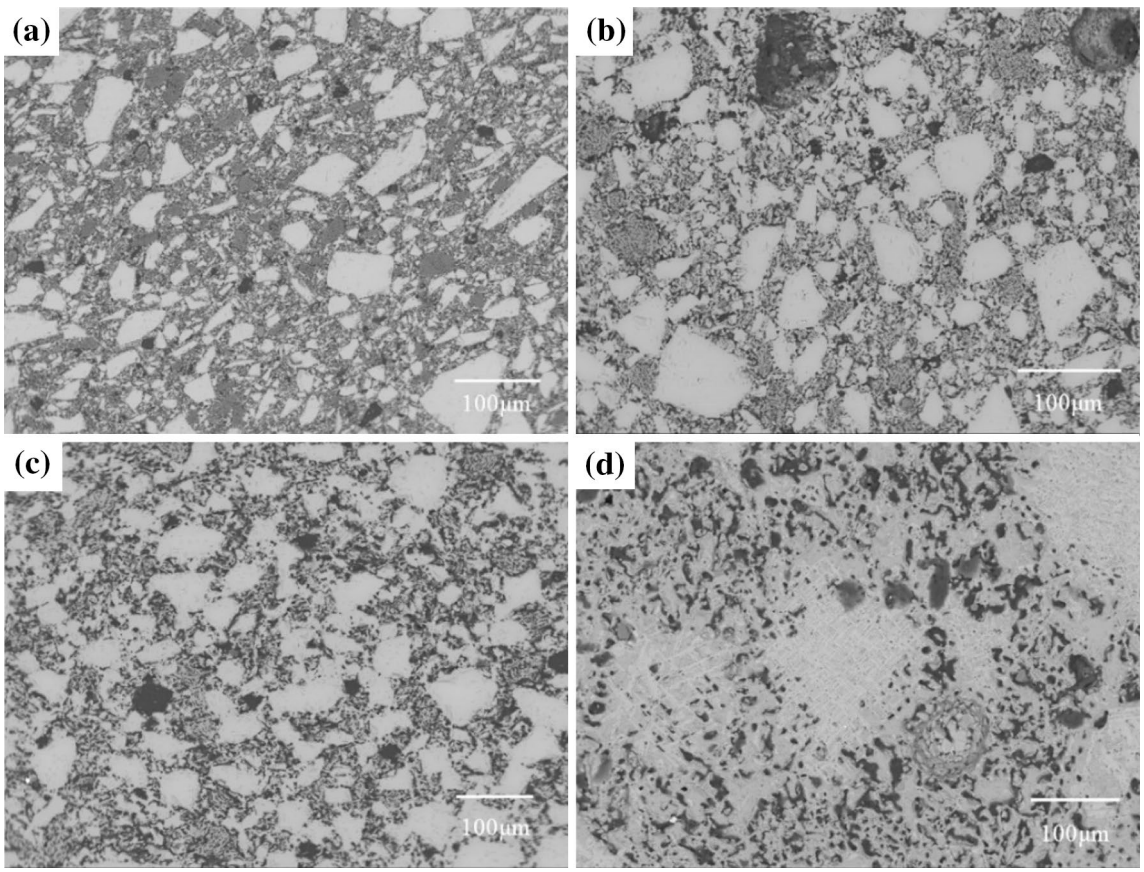


**Fig. 6** Microstructure of Al-rich sample heated at 1200 °C (**a**), 1300 °C (**b**), 1400 °C (**c**) and 1500 °C (**d**)

occurring. With temperature rising, the edge of the particles becomes a little smooth (Fig. 6b) due to the diffusion of ions. This phenomenon becomes much more obvious above 1400 °C (Fig. 6c, d).

The element map scanning of Al-rich sample heated at 1200 and 1400 °C was analyzed, respectively. After heated at 1200 °C, the distribution of Mg is relatively homogeneous due to its low concentration (Fig. 7a). There are some Al enrichment areas, indicating that a large proportion of $Al_2O_3$ added does not react and exists as a single phase. This is in agreement with the XRD result shown in Fig. 5b. After heated at 1400 °C, the distribution of Al becomes uniform

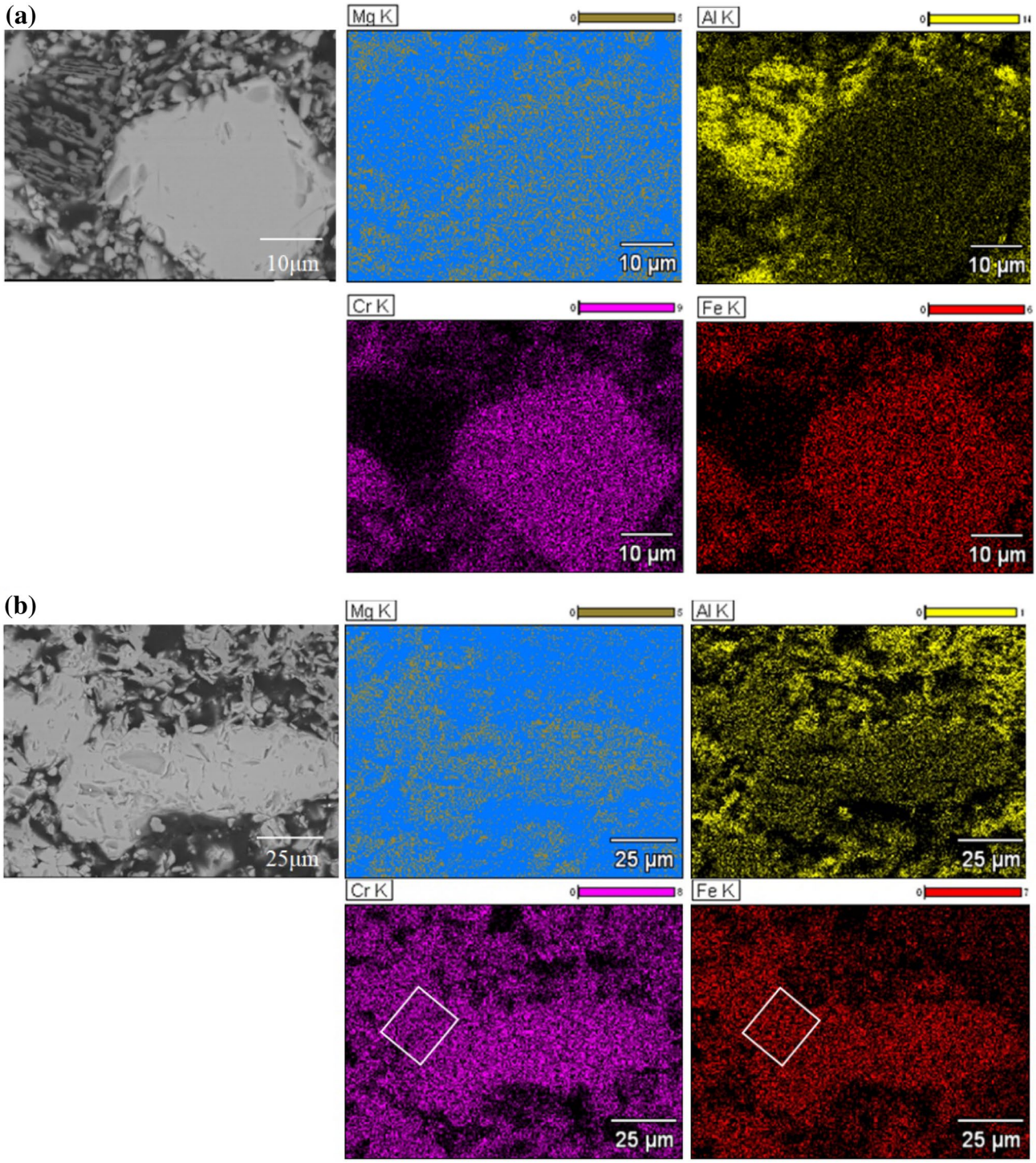


**Fig. 7** Element map scanning of Al-rich sample heated at 1200 °C (**a**) and 1400 °C (**b**)

(Fig. 7b). The reaction between chromite and $Al_2O_3$ occurs where they are in contact [18] and Al-rich sesquioxide is formed due to the excess sesquioxide on the surface layer of chromite grains. The distribution of Fe in contact position is a little richer compared with that of Cr shown in the rectangle region, indicating that the diffusion of Fe contributes to the connection between chromite particles.

### 4.3 Physical properties of sample sintered at different temperatures

The linear change ratio of the sinter sample is shown in Fig. 8a. Linear change ratio tends to increase with rising temperature, which is related to the densification. By comparison, Mg-rich sample shows less linear change ratio than Al-rich sample due to the formation of more spinel phase in Mg-rich sample [6]. Figure 8b shows the cold strength of Mg-rich and Al-rich samples heated at different temperatures; the cold strength of both Mg-rich and Al-rich samples was found to increase with increasing sintering temperature. The fracture position is in the inner of chromite at 1600 °C and in the gap between chromite grains at 1200 °C shown in Fig. 9, indicating that the bonding strength between chromite increases with rising temperature further. The high cold strength of Mg-rich and Al-rich samples heated at 1600 °C is probably due to its composite polymineral structure, well developed interphase boundaries and the presence of the sesquioxide phase which reacts as a reinforcing component [13]. Cold strength of Al-rich sample is higher than that of Mg-rich sample in general, which may be due to the higher content of sesquioxide in Al-rich sample.

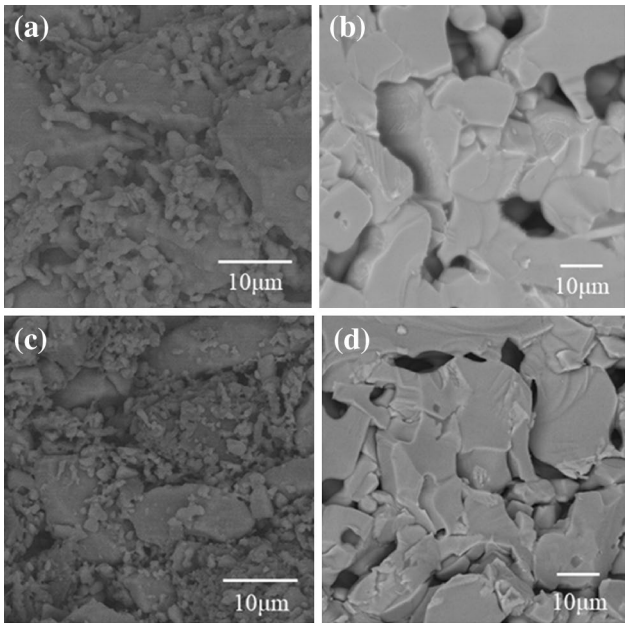


**Fig. 9** Microstructure of fracture surface of Mg-rich sample heated at 1200 °C (**a**) and 1600 °C (**b**) as well as Al-rich sample heated at 1200 °C (**c**) and 1600 °C (**d**)

### 4.4 Sintering mechanism

From the above analysis, the reaction process of chromite by adding MgO and $Al_2O_3$ can be proposed as follows. At low temperature, $Fe^{2+}$ ions diffuse from the core of chromite grains toward the surface and are oxidized into $Fe^{3+}$, forming $Fe_2O_3$ on the surface of chromite. Then, MgO and $Al_2O_3$ diffuse into the surface of chromite to form complex $Mg(Fe,Al)_2O_4$ spinel at 1200 °C shown in Fig. 2b. However,

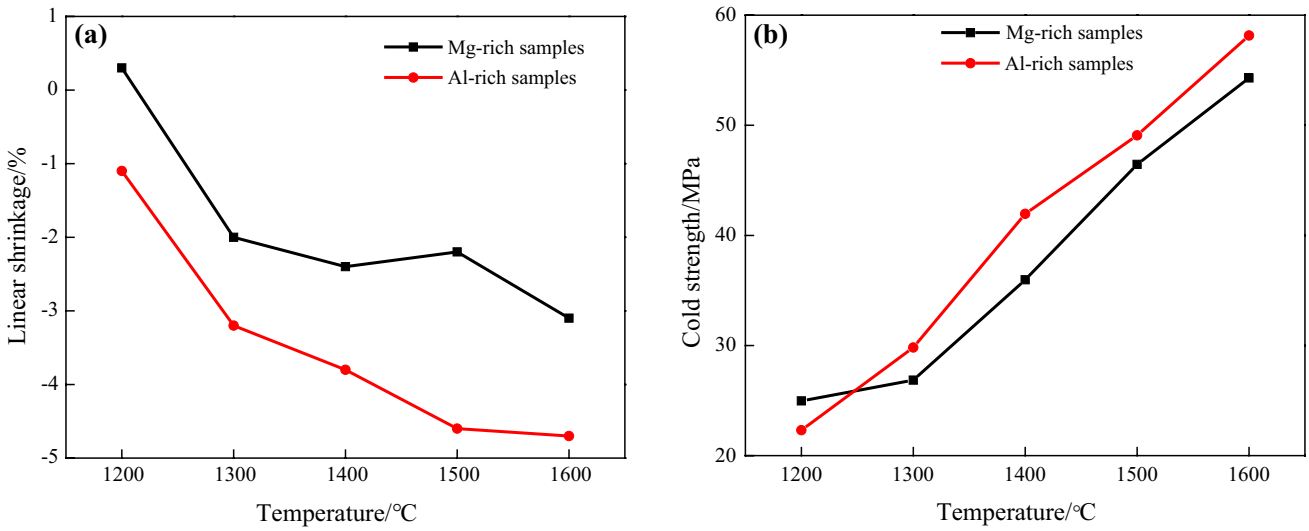


**Fig. 8** Linear change ratio (**a**) and cold rupture strength (**b**) of Mg-rich and Al-rich samples heated at different temperatures

the diffusion rate is slow due to the low temperature. As temperatures rises, the diffusion of MgO into chromite is accelerated and more $Mg(Fe,Al)_2O_4$ spinel is formed. As temperature further increases, MgO added further diffuses into chromite, occupying the tetrahedral vacancies, which will stabilize the spinel structure. Due to the high diffusion rate of $Mg^{2+}$ ions, $Mg^{2+}$ ions have diffused into the chromite, occupying the tetrahedral vacancies. Due to the low diffusion rate of $Al^{3+}$ ions, the diffusion distance of $Al^{3+}$ ions is limited and $Al^{3+}$ ions mainly exist on the surface layer of chromite grains. Therefore, on the surface layer, there exists excess sesquioxide phase that will form the

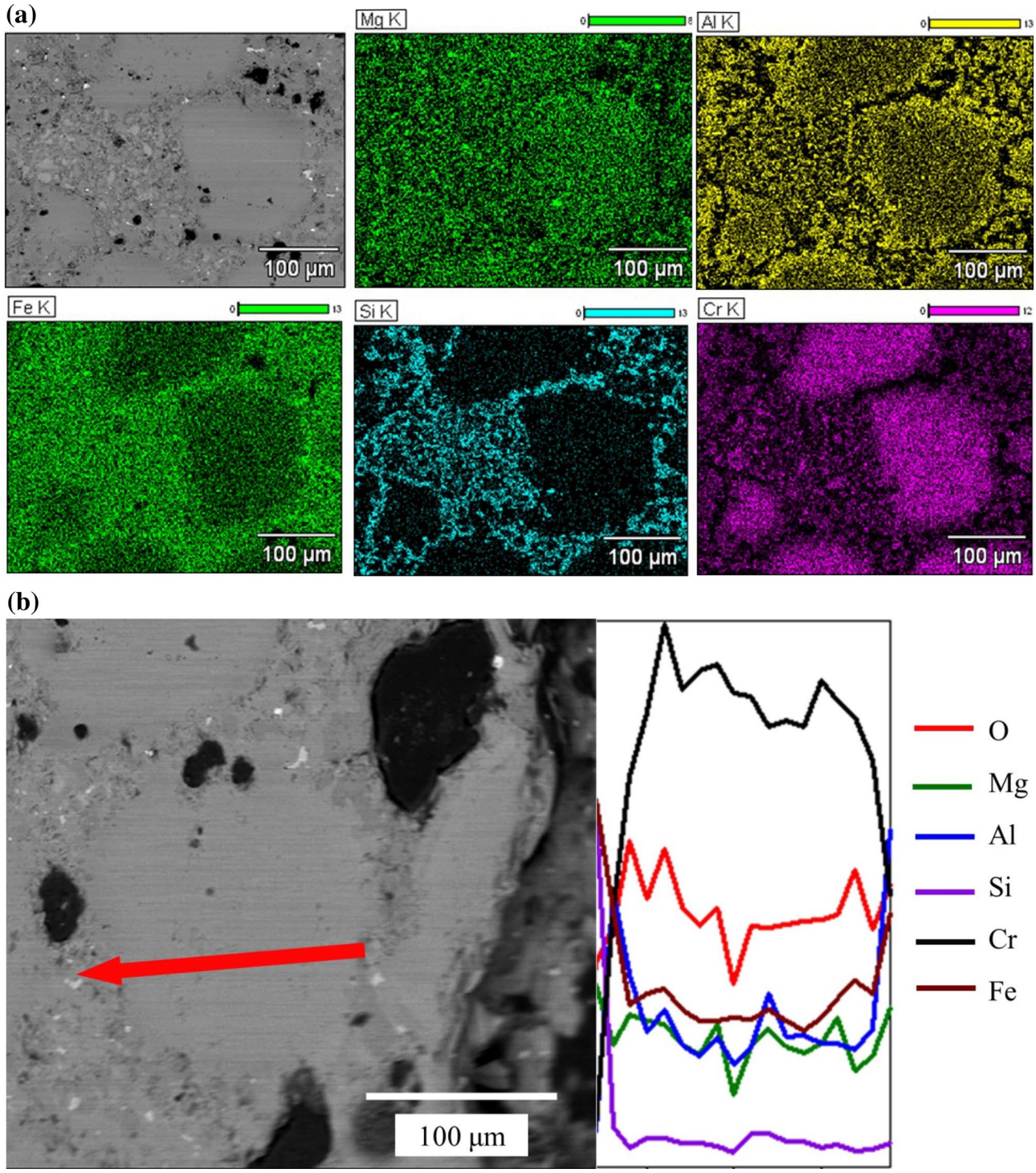


**Fig. 10** Illustration of chemical degradation mechanism of Mg-rich sample through interaction with a fayalite slag. **a** Map scanning of single chromite particle eroded; **b** line scanning for single chromite particle eroded

spinel-sesquioxide structure, which has been verified by XRD and SEM analysis. It can be predicted that the thermal shock resistance of Mg-rich and Al-rich samples is superior due to the presence of multiphase microstructure possessing different thermal expansion [19].

### 4.5 Slag resistance

In order to test the property of samples against fayalite slag, the chemical degradation of Mg-rich and Al-rich samples interacting with fayalite slag is carried out. In this

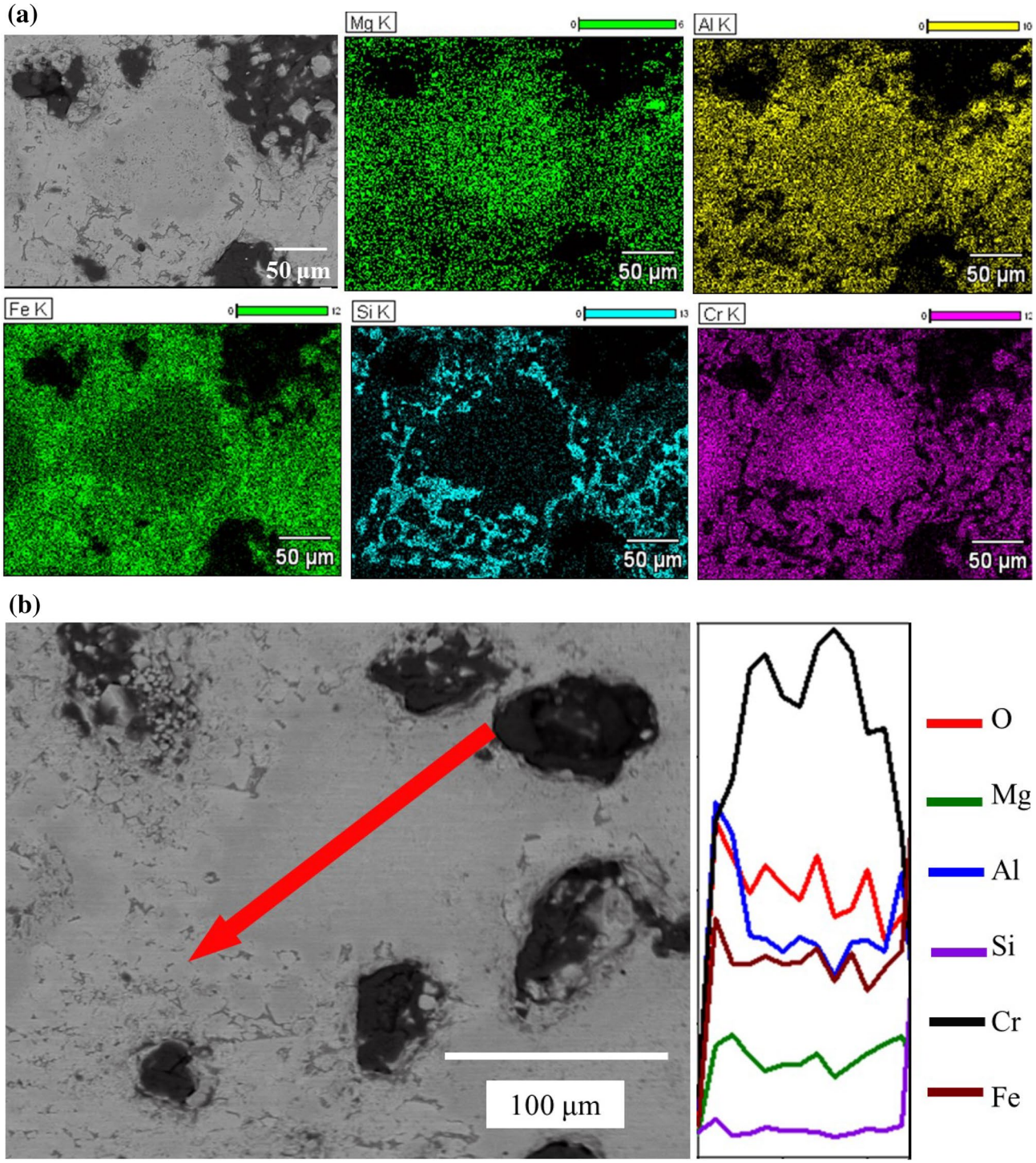


**Fig. 11** Illustration of chemical degradation mechanism of Al-rich sample through interaction with a fayalite slag. **a** Map scanning of single chromite particle eroded; **b** line scanning of single chromite particle eroded

experiment, the crucible possesses a loose and porous structure to ensure the full reaction of slag and chromite particles, aiming to investigate the reaction between slag and chromite particles. The reaction between Mg-rich sample and fayalite slag is shown in Fig. 10a. It can be seen that the pores between chromite particles have been occupied by the reaction products. The wide distribution of Mg in the slag indicates that $Mg^{2+}$ ions in chromite are substituted by $Fe^{2+}$ ions in slag. There is an Al- and Si-rich ring around chromite particle. The concentration of Fe in chromite is much lower than that in slag, indicating that Fe in slag hardly diffuses into chromite. Figure 10b shows the line scanning of single chromite particle reacted with fayalite slag, and the contents of Fe and Al in the surface of chromite are higher than those in the core of chromite, further indicating that a layer rich in Fe and Al is formed. This layer can prevent the further diffusion of Fe from slag toward chromite. Thus, the corrosion resistance of fayalite slag is improved [20].

Figure 11 shows the chemical degradation of Al-rich sample through interaction with fayalite slag. The macrograph of single chromite grain after reaction is shown in Fig. 11a, b. The pores between chromite particles are occupied, forming a dense structure which can block the infiltration channel. The content of Fe on the surface of chromite is higher than that in chromite and the content of Mg in the core of chromite is higher than that on the surface, indicating that the interdiffusion of Fe and Mg between slag and chromite is blocked. The contents of Fe and Al on the surface of chromite are higher than those in the core of chromite, indicating that a protective layer rich in Fe and Al is formed, which is beneficial for the corrosion resistance improvement. Compared with Mg-rich sample shown in Fig. 11a, Mg ions have been substituted by Fe ions widely and Al-rich sample maintains high concentration of Mg in chromite. This phenomenon can be explained by the component difference. As for Mg-rich sample, the amount of sesquioxide phase is less because of the excess addition of MgO, which can be seen from Fig. 2a that the peak of sesquioxide phase is hard to be detected. As for Al-rich sample, the amount of sesquioxide phase is adequate because of the excess addition of $Al_2O_3$, and the spinel-sesquioxide structure is well developed. Hence, Al-rich sample shows better corrosion resistance toward fayalite slag.

## 5 Conclusion

The phase and morphological development of chromite during sintering are investigated by introducing MgO and $Al_2O_3$ as additives in the temperature range of 1200–1600 °C in air. At low temperature, the diffusion rates of MgO and $Al_2O_3$ are slow, and these two additives hardly react with the chromite grains. However, the diffusion rate is accelerated with rising temperatures. Above 1500 °C, MgO diffuses into chromite, occupying the tetrahedral vacancies caused by the diffusion and oxidation of Fe to stabilize the spinel structure, while $Al_2O_3$ diffuses into the surface layer of chromite to form the spinel-sesquioxide structure. After structure optimization, the chromite shows excellent corrosion resistance toward fayalite slag. The existence of sesquioxide phase near the surface blocks the interdiffusion between $Fe^{2+}$ in slag and $Mg^{2+}$ in chromite.

**Acknowledgements** The authors express their appreciations to the National Natural Science Foundation for Excellent Young Scholars of China (No. 51522402), the National Natural Science Foundation of China (Nos. 51904021 and 51974021) and Fundamental Research Funds for the Central Universities (No. FRF-TP-19-008A1) for financial support.

## References

[1] A. Azhari, F. Golestani-Fard, H. Sarpoolaky, J. Eur. Ceram. Soc. 29 (2009) 2679–2684.
[2] K. Goto, Shigen-Chishitsu 47 (1997) 223–229.
[3] H. Zargar, Sintering studies of magnesia-chromite refractory composites, University of British Columbia, Canada, 2014.
[4] M.L. Van Dreser, W.H. Boyer, J. Am. Ceram. Soc. 46 (1963) 257–264.
[5] D.H. Speidel, J. Am. Ceram. Soc. 50 (1967) 243–248.
[6] K.X. Chen, Y. Li, Z.H. Huang, J. Northwest Inst. Light Ind. (1992) No. 3, 151–155.
[7] A. Malfliet, S. Lotfian, L. Scheunis, V. Petkov, L. Pandelaers, P. T. Jones, B. Blanpain, J. Eur. Ceram. Soc. 34 (2014) 849–876.
[8] X.W. Zhu, W.D. Qiu, Y.H. Liang, W. Zhao, P. Yue, J.H. Nie, R.Q. Cui, Refractories 47 (2013) 430–432.
[9] S. Asano, Taikabutsu 42 (1990) 341–342.
[10] V.D. Tathavakar, M.P. Antony, A. Jha, Metall. Mater. Trans. B 36 (2005) 75–84.
[11] P.E. Scheerer, H.M. Mikami, J.A. Tauber, J. Am. Ceram. Soc. 47 (1964) 297–305.
[12] H.G. Emblem, T.J. Davies, A. Harabi, A.A. Ogwu, C.S. Nwobodo, V. Tsantzalou, J. Mater. Sci. Lett. 11 (1992) 820–821.
[13] G.M. Dodis, T.V. Dodis, P.N. Babin, Refractories 23 (1982) 25–30.
[14] W.S. Treffner, J. Am. Ceram. Soc. 44 (1961) 583–591.
[15] S.M. Zubakov, Refractories and Industrial Ceramics 1 (1960) 220–225.
[16] D. Zhu, C. Yang, J. Pan, X.B. Li, Metall. Mater. Trans. B 47 (2016) 2919–2930.
[17] J. Pan, C.C. Yang, D.Q. Zhu, ISIJ Int. 55 (2015) 727–735.
[18] R.E. Carter, J. Am. Ceram. Soc. 44 (1961) 116–120.
[19] M.K. Haldar, H.S. Tripathi, S.K. Das, A. Ghosh, Ceram. Int. 30 (2004) 911–915.
[20] J.R. Donald, J.M. Toguri, C. Doyle, Metall. Mater. Trans. B 29 (1998) 317–323.